Chemical Physics xxx (xxxx) 111631

Contents lists available at ScienceDirect

Chemical Physics

journal homepage: www.elsevier.com/locate/chemphys

Hydrogen/deuterium exchange in 1-alkyl-3-methylimidazolium bis(trifluoromethanesulfonyl)imide-based solutions

Hiroshi Abe *, Yuto Yoshiichi, Hiroaki Kishimura

Department of Materials Science and Engineering, National Defense Academy, Yokosuka 239-8686, Japan

ARTICLE INFO

Keywords:
Hydrogen/deuterium exchange
Ionic liquids
Alkyl chain length dependence
Molecular conformation

ABSTRACT

Here, hydrogen/deuterium (H/D) exchange in hydrophobic ionic liquid (IL)-propanol solutions were investigated by Raman spectroscopy. The ILs were 1-alkyl-3-methylimidazolium bis(trifluoromethanesulfonyl)imide, [$C_n$mim][TFSI] (n = 2–6). Fully deuterated methanol (MeOD-d_4), acetone-d_6, and 2-propanol (2-PrOD-d_8) were used. H/D exchange was not observed in [C_2mim][TFSI]-based mixtures. The constant fraction of D over the entire concentration range of 2-PrOD-d_8 studied was observed in [C_3mim][TFSI]-based mixtures. The distinct H/D exchange in [C_4mim][TFSI]-based mixtures was dependent on the 2-PrOD-d_8 concentration. The H/D exchange had no cationic alkyl chain length dependencies. Kinetic H/D exchange depended on the types of additives.

1. Introduction

Hydrogen/deuterium (H/D) exchange has been investigated using Raman [1,2] and nuclear magnetic resonance (NMR) [3,4] spectroscopy. Molecular conformations are typically related with the H/D exchange fractions. H/D exchange mass spectroscopy (HDX-MS) has been utilized as a powerful tool to clarify the folding dynamics of proteins [5–9]. The interaction sites of a protein complex were determined by the HDX-MS by monitoring the exchange rate.

Ionic liquids (ILs) have been applied as green materials in CO_2 capture [10,11], catalysts [12,13], and electrochemical devices [14–16]. Various ILs have been designed by changing the combinations of cations and anions. 1-Alkyl-3-methylimidazolium ([$C_n$mim]$^+$) is regarded as a representative cation in ILs, where n is the alkyl chain length. H/D exchange in IL-based mixtures has been observed by NMR and Raman spectroscopy [17–28]. Particularly in [$C_n$mim][X]-D_2O, the H/D exchange occurred in the second carbon of the cation (C(2)-H ••• D-O-D → C(2)-D ••• H—O—D). In Raman spectroscopy, the H/D exchange was distinguished by the peak area ratio of Raman bands at 1010 and 1024 cm^{-1}, which were attributed to C(2)-D and C(2)-H, respectively [21–23]. Kinetic H/D exchange of [C_{10}mim][X]-D_2O using Raman spectroscopy was comparable to NMR [22]. In [C_4mim][X], the H/D exchange was also examined systematically by Raman spectroscopy [23]. The *trans* and *gauche* conformers of the [C_4mim]$^+$ cation were dependent on the H/D exchange fractions. Moreover, it has been found that fully equilibrated H/D exchange fractions are influenced by the types of anions [23]. On the D_2O concentration scale, the H/D exchange of [C_4mim][X] was classified as extended-N shape ([BF_4]$^-$), extended-S shape (Cl^-, SCN^-, and CH_3COO^-), linear shape ([PF_6]$^-$), and none ([NO_3]$^-$). In [C_4mim][NO_3]-D_2O, the H/D exchange was completely suppressed even for 58 days [29]. In contrast, the H/D exchange in [C_6mim][NO_3]-D_2O was faster (i.e., finished within 2hrs) [28]. In systematic experiments using [$C_n$mim][NO_3] (n = 2, 4, 6, and 8), only [C_6mim][NO_3]-D_2O showed a distinct H/D exchange.

Hydrophobic 1-alkyl-3-methylimidazolium bis(trifluoromethanesulfonyl)imide ([$C_n$mim][TFSI]) is freely soluble in alcohols [30,31]. In the liquid–liquid equilibria (LLE) of [$C_n$mim][TFSI]-alcohol, an alcohol isomer effect was observed markedly. Moreover, conformers of the [TFSI]$^-$ anion varied, depending on the types of alcohol isomers and alcohol concentration. The [TFSI]$^-$ anion has two stable conformers, namely *cis* (C_1) and *trans* (C_2). Moreover, the liquid structures of pure [$C_n$mim][TFSI] have been examined by small- and wide-angle X-ray scattering (SWAXS) [32]. In ILs with $n \geq 6$, nanoheterogeneity of pure [$C_n$mim][TFSI] developed proportionally to the alkyl chain length. Furthermore, propanol isomer effect in [$C_n$mim][TFSI] has been obtained by SWAXS [33]. Critical scattering that was derived from a phase separation coexisted in the prepeak. This revealed the nanoheterogeneity in the mixtures.

In this study, H/D exchange of hydrophobic [$C_n$mim][TFSI]-deuterated methanol (MeOD-d_4), acetone-d_6, and 2-propanol (2-PrOD-d_8) solutions were examined by Raman spectroscopy. The cation effect in the H/D exchange was distinguished by changing the alkyl chain length of the [$C_n$mim]$^+$ cations. The types of H/D exchange fractions

* Corresponding author.
E-mail address: ab@nda.ac.jp (H. Abe).

https://doi.org/10.1016/j.chemphys.2022.111631
Received 23 March 2022; Received in revised form 27 June 2022; Accepted 28 June 2022
0301-0104/© 20XX

UNCORRECTED PROOF

Note: Low-resolution images were used to create this PDF. The original images will be used in the final composition.

were classified as a function of 2-PrOD-d_8 concentration. Additive effect was also observed in the kinetic H/D exchange.

2. Experimental

The ILs used in this study are hydrophobic [$C_n$mim][TFSI] (n = 2–6). The second carbon (C(2)) of the [$C_n$mim]$^+$ in Fig. 1 is the H/D exchange site. The [TFSI]$^-$ possesses two stable conformers, namely *cis* (C_1) and *trans* (C_2) as shown in Fig. 1. [C_4mim][TFSI] was purchased from Kanto Chemical Co. (Tokyo, Japan). The other [$C_n$mim][TFSI] (n = 2, 3, 5, and 6) were obtained from IoLiTec GmbH. The additives used were non-deuterated 2-propanol (2-PrOH) from Kanto Chemical Co., MeOD-d_4 and 2-PrOD-d_8 from Acros Organics, and acetone-d_6 from Cambridge Isotope Laboratories. In the same manner with the previous study [30], clouding and phase separations did not occur at room temperature in [$C_n$mim][TFSI] (n = 2–6) based mixtures. We obtained the Raman spectra of fully equilibrated mixtures, which were stored at room temperature for ~ 48hrs after mixing. In the kinetic experiments, we started to count time just after mixing.

An NRS-5100 Raman Spectrometer from JASCO Co., which was equipped with a monochromator and Peltier-cooled camera was used. The excitation was triggered by a 5.8 mW green laser with wavelength of 532 nm.

3. Results and discussion

3.1. H/D exchange of [C_2mim][TFSI]-2-PrOD-d_8 and [C_3mim][TFSI]-2-PrOD-d_8

H/D exchange rate by Raman spectroscopy is typically determined by the two bands at 1010 and 1024 cm^{-1} for C(2)-D and C(2)-H, respectively [21,23]. In [C_2mim][TFSI]-2-PrOD-d_8, the C(2)-D signal was not observed in all the propanol concentrations studied (Fig. 2). Therefore, the H/D exchange was suppressed completely in the [C_2mim][TFSI]-based mixtures. Previously, critical scattering in [C_2mim][TFSI]-propanol was observed by SWAXS [33]. Therefore, we deduced that additional fluctuations could interrupt the H/D exchange.

Meanwhile, partial H/D exchange was observed in [C_3mim][TFSI]-2-PrOD-d_8 (Fig. 3). Notably, the Raman peak area ratio was consistent at 2-PrOD-d_8 concentrations of 10–98 mol%. Almost constant and incomplete HD exchange were observed initially in the IL-based mixtures. For quantitative analysis, the H/D exchange fraction (f_D) is introduced and given by equation (1).

$$f_D = \frac{I_D}{I_H + I_D} \quad (1)$$

Where, I_H and I_D are the peak areas of C(2)-H and C(2)-D Raman bands, respectively. The observed Raman bands were decomposed using an asymmetric pseudo-Voigt profile fitting. In the f_D plot of the [C_3mim][TFSI]-based system (Fig. 4), a constant f_D was observed at all the propanol concentrations. Compared with [C_4mim][X]-D_2O in a previous study [23], the f_D tendency of [C_3mim][TFSI]-2-PrOD-d_8 was not

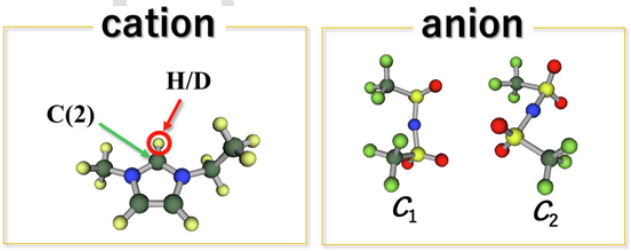

Fig. 1. Molecular structures of [C_2mim]$^+$ and [TFSI]$^-$. H/D exchange occurs at the C(2) of the [C_2mim]$^+$. [TFSI]$^-$ has two conformers, namely *cis* (C_1) and *trans* (C_2).

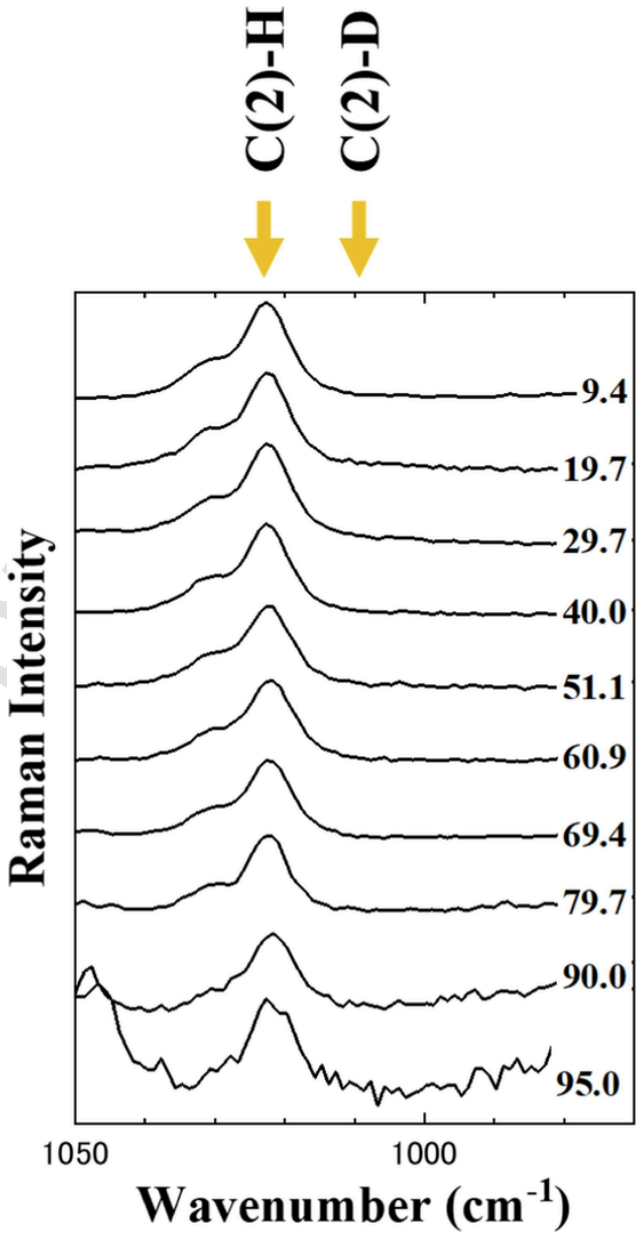

Fig. 2. No H/D exchange on Raman bands of [C_2mim][TFSI]-2-PrOD-d_8. The 1010 and 1024 cm^{-1} Raman bands are caused by C(2)-D and C(2)-H, respectively. These Raman bands are indicated by the arrows. Numbers in the figure reveal × mol% 2-PrOD-d_8.

extended-N shape ([BF_4]$^-$), extended-S shape (Cl^-, SCN^-, and CH_3COO^-), linear shape ([PF_6]$^-$), or none ([NO_3]$^-$) (Table 1). On the other hand, [C_6mim][NO_3]-D_2O indicated full H/D exchange at $10 \le x \le 98$ mol%. Thus, the constant f_D values were classified into three types: f_D = 0 of [$C_n$mim][NO_3]-D_2O (n = 2, 4, and 8); f_D ~ 0.2 of [C_3mim][TFSI]-2-PrOD-d_8; and f_D = 1 of [C_6mim][NO_3]-D_2O (Table 1). Cationic conformational degrees of freedom are changed generally by the alkyl chain length. Since constant f_D appeared at n = 2, 3, 5, and 6 of the [$C_n$mim][TFSI]-2-PrOD-d_8, the constant f_D values were not derived from the conformations of the [$C_n$mim]$^+$ cations. Furthermore, the constant f_D type was not connected with liquid structures, which are quite sensitive to water or propanol concentrations [33].

ARTICLE IN PRESS

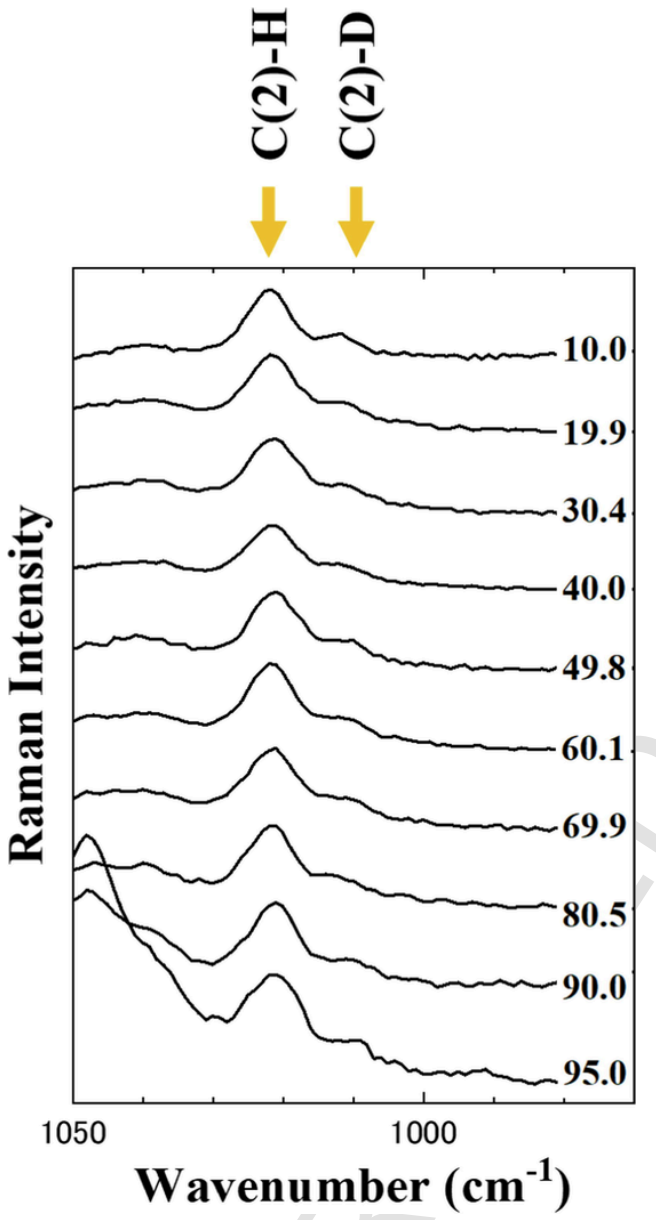

Fig. 3. H/D exchange on the Raman bands of [C_3mim][TFSI]-2-PrOD-d_8. Constant H/D exchange fraction appeared at the entire propanol concentration range. These Raman bands are indicated by the arrows. Numbers in the figure reveal × mol% 2-PrOD-d_8.

3.2. H/D exchange of [C_4mim][TFSI]-2-PrOD-d_8

The Raman bands obtained for [C_4mim][TFSI]-2-PrOD-d_8 are shown in Fig. 5. With the increase in propanol concentration, the C(2)-D and C(2)-H Raman intensities increased and decreased, respectively. Thus, the H/D exchange was influenced extensively by the propanol concentration. In the f_D plot shown in Fig. 4, [C_4mim][TFSI]-2-PrOD-d_8 showed a linear shape such as [C_4mim][PF_6]-D_2O in Table 1 [23], suggesting that the H/D exchange rate was proportional to the number of propanol molecules, which surrounded the [C_4mim]$^+$ cation. However, the linear f_D was restricted at $<$ 40 mol% D_2O at room temperature for [C_4mim][PF_6] (Table 1) [23]. This was explained by the phase separation in [C_4mim][PF_6]-D_2O at $>$ 40 mol% at room temperature.

Stable *gauche* and *trans* confirmers in the liquid state exist in the [C_4mim]$^+$ cation [23]. The 600 and 620 cm^{-1} Raman bands were assigned to the *gauche* and *trans* conformers, respectively. Both Raman bands varied depending on the propanol concentration (Fig. 6). It has been noticed that the conformer ratio in hydrophobic IL-non-deuterated propanol solutions was affected by the amount of non-deuterated propanol additives [30,31,34]. Thus, we obtained the Raman spectra of [C_4mim][TFSI]–non-deuterated 2-propanol (2-PrOH). For quantitative comparison, the peak area ratio of *gauche* to *trans* (I_{gauche}/I_{trans}) was calculated after a peak profile fitting. The I_{gauche}/I_{trans} values of [C_4mim][TFSI]-2-PrOH are summarized in Fig. S1(a). At 2-PrOH concentrations of $<$ 90 mol%, the I_{gauche}/I_{trans} was almost constant (Table 2). At concentrations of $>$ 90 mol%, the peak area ratio in-

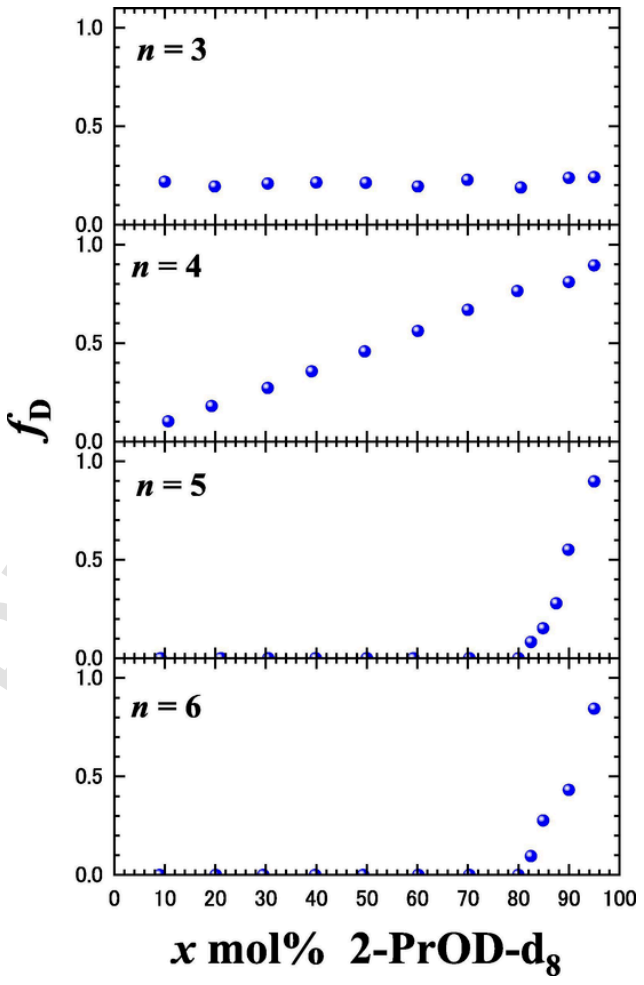

Fig. 4. H/D exchange fraction, f_D, as × mol% 2-PrOD-d_8 in [$C_n$mim][TFSI] (n = 3, 4, 5, and 6). Constant f_D was observed in [C_3mim][TFSI]-2-PrOD-d_8.

Table 1
Classification of H/D exchanges in IL-based solutions. Constant & linear represents that constant f_D appeared in the 2-PrOD-d_8 poor region and linear increase of f_D was observed in the 2-PrOD-d_8 rich region.

f_D type	Hydrophilic IL-D_2O	Hydrophobic IL-2-PrOD-d_8
Extend-N	$[BF_4]^-$	[23]
Extend-S	Cl^-, SCN^-, CH_3COO^-	[23]
Linear		
low x	$[PF_6]^-$	[23]
whole x		[C_4mim][TFSI]
Constant		
f_D = 0	[$C_n$mim][NO_3] (n = 2, 4, and 8)[28]	[C_2mim][TFSI]
f_D ~ 0.2	[C_3mim][TFSI]	
f_D = 1	[C_6mim][NO_3]	[28]
Constant	[$C_n$mim][TFSI] (n = 5 and 6)	& Linear

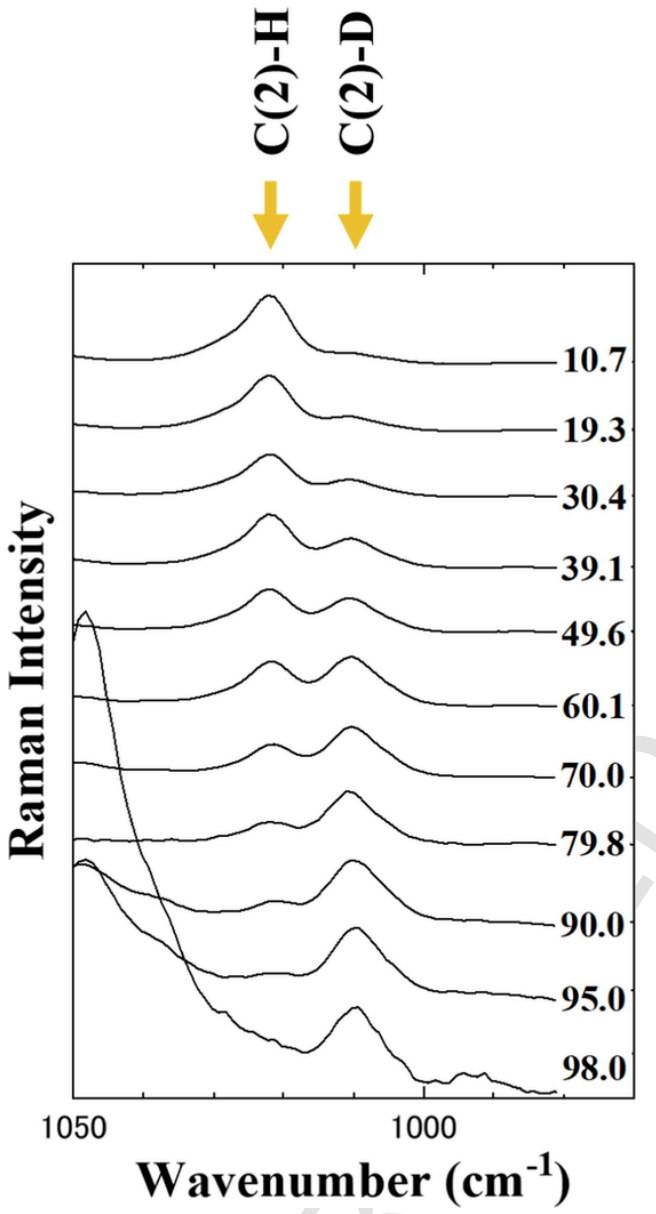

Fig. 5. H/D exchange on the Raman bands of $[C_4mim][TFSI]$-2-PrOD-d_8. H/D exchange was pronounced at higher concentrations of propanol. These Raman bands are indicated by the arrows. Numbers in the figure reveal × mol% 2-PrOD-d_8.

creased slightly with increasing concentration. Meanwhile, I_{gauche}/I_{trans} of $[C_4mim][TFSI]$-2-PrOD-d_8 showed a different behavior with 2-PrOD-d_8 concentration as shown in Fig. S1(b). The I_{gauche}/I_{trans} values varied at 0.7–1.9 with increasing 2-PrOD-d_8 concentration. It should be noticed that, focusing on the additive concentration dependency, the I_{gauche}/I_{trans} of $[C_4mim][TFSI]$-2-PrOD-d_8 was similar to that of $[C_4mim][BF_4]$-D_2O classified as extended-N shape (Table 2) [23]. This implies that the cation conformers in $[C_4mim][TFSI]$-2-PrOD-d_8 are influenced by nanoheterogeneous liquid structure, similarly to those in $[C_4mim][BF_4]$-D_2O. By small-angle neutron scattering, fluctuations derived from phase separation were enhanced in the center of $[C_4mim][BF_4]$-92.5 mol% D_2O [35]. The different I_{gauche}/I_{trans} between $[C_4mim][TFSI]$-2PrOH and −2-PrOD-d_8 (Table 2) could be originated from the different of the LLEs.

The $[TFSI]^-$ is characterized by the degrees of freedom of its conformers as shown in Fig. 1. Raman bands denoted by C_1 and C_2 in Fig. 7 are for the *cis* and *trans* conformers of the $[TFSI]^-$ anion, respectively.

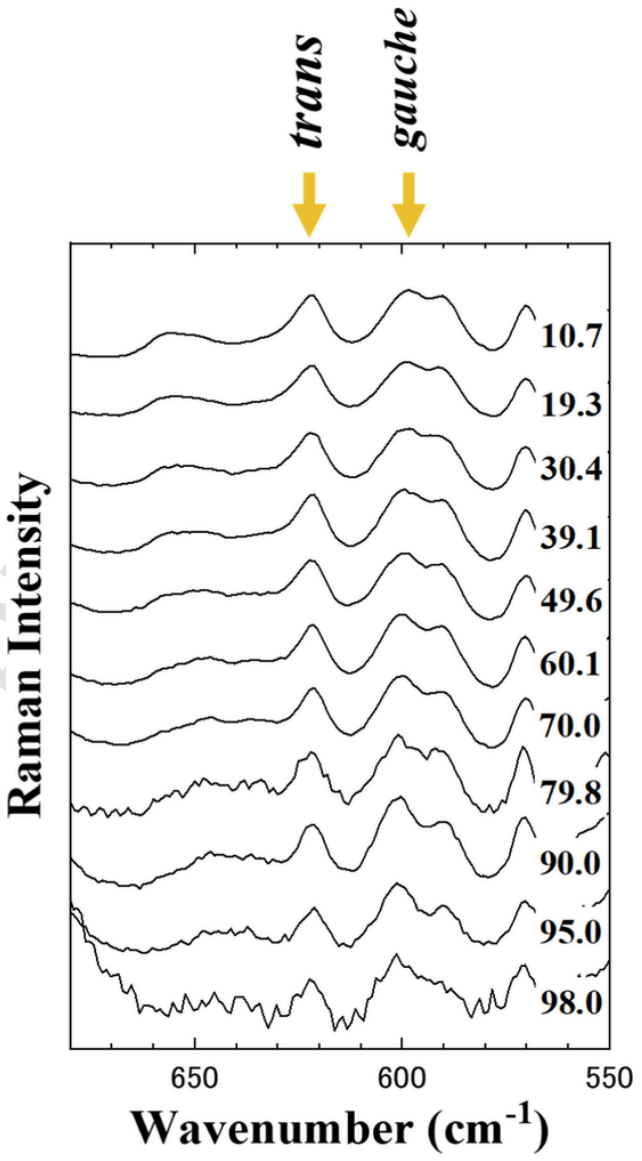

Fig. 6. × mol% 2-PrOD-d_8 dependence of *gauche* and *trans* conformers of $[C_4mim]^+$. These Raman bands are indicated by the arrows. Numbers in the figure reveal × mol% 2-PrOD-d_8.

Table 2
Types of H/D exchange relating to cation and anion effects in hydrophilic $[C_4mim][BF_4]$-D_2O and hydrophobic $[C_4mim][TFSI]$-2-PrOD-d_8. For a comparison, the cation and anion effects of $[C_4mim][TFSI]$-2-PrOH is noted.

	f_D	I_{gauche}/I_{trans} (cation)	C_2/C_1 (anion)
$[C_4mim][BF_4]$-D_2O	Extended-N shape	Extended-N shape	–
$[C_4mim][TFSI]$-2-PrOH	–	Constant	Inverse-S shape
$[C_4mim][TFSI]$-2-PrOD-d_8	Liner shape	Extended-N shape	Inverse-S shape

By the density functional theory (DFT) calculations [36], the C_1 and C_2 conformers were identified. The C_2/C_1 ratios of hydrophobic IL-propanol solutions have been measured by Raman spectroscopy [31,34,37]. The C_2/C_1 ratios were modified by additives such as 1-PrOH and 2-PrOH. The 325 and 339 cm^{-1} Raman bands were attributed to the C_1 and C_2 conformers of $[TFSI]^-$, respectively [38]. To distinguish the H/D exchange from propanol additive effects, we obtained the Raman spec-

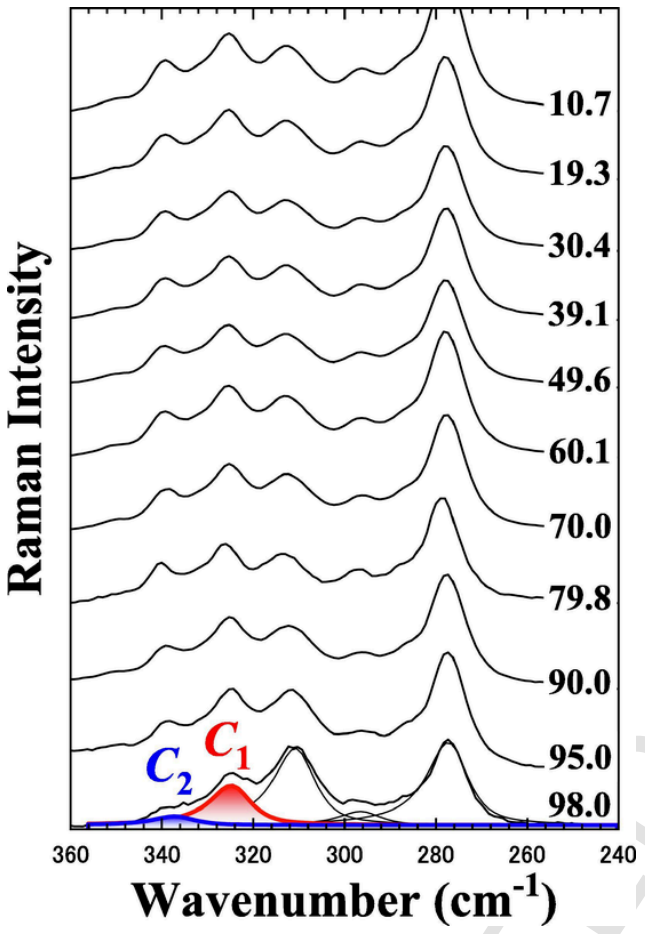

Fig. 7. × mol% 2-PrOD-d_8 dependence of *cis* (C_1) and *trans* (C_2) of $[TFSI]^-$. Numbers in the figure reveal × mol% 2-PrOD-d_8.

tra for 2-PrOH- and 2-PrOD-d_8-based mixtures. The C_2/C_1 ratio of [C_4mim][TFSI]-2-PrOH is shown in Fig. S2(a). The C_2/C_1 ratios decreased slightly at 2-PrOH concentrations of < 80 mol%. The ratios then decreased drastically at concentrations > 90 mol%. Here, the C_2/C_1 ratio curve is named as inverse-S shape (Table 2). In [C_4mim][TFSI]-2-PrOD-d_8, slightly different C_2/C_1 behaviors were observed as shown in Fig. S2(b). At 2-PrOD-d_8 concentrations of < 60 mol%, the C_2/C_1 values were almost constant. The decrease in the C_2/C_1 values at 2-PrOD-d_8 concentrations of > 90 mol% was similar to 2-PrOH at the same concentrations. Thus, the C_2/C_1 of [C_4mim][TFSI]-2-PrOD-d_8 is also classified to the same group (inverse-S shape). Since the C_2/C_1 behaviors in both systems were similar, $[TFSI]^-$ cannot contribute to the H/D exchange. Thus, the main contribution for the H/D exchange could be the cation effect in [C_4mim][TFSI]-2-PrOD-d_8. In the previous study [33], the observed C_2/C_1 values implied solution stability. The C_2 conformer of $[TFSI]^-$ has been found to be more stable than C_1 by the DFT calculation of [$C_n$mim][TFSI]-2-PrOH. In the [C_4mim][TFSI]-98 mol% 2-PrOD-d_8 mixture, the C_2/C_1 value was small (i.e., 0.22); thus, an unstable liquid state was realized in the propanol-rich region.

Linear shape of f_D as shown in Fig. 4 appeared in [C_4mim][TFSI]-2-PrOD-d_8, although I_{gauche}/I_{trans} was extended-N shape (Fig. S1(b)). In case of [C_4mim][BF_4]-D_2O [23], extended-N shape of f_D coincided with that of I_{gauche}/I_{trans}. The discrepancy between [C_4mim][BF_4]-D_2O and [C_4mim][TFSI]-2-PrOD-d_8 implies that some additional factor for H/D exchange effect could be superimposed to [C_4mim][TFSI]-2-PrOD-d_8. In [$C_n$mim][TFSI]-2-PrOD-d_8 (n = 4, 5, and 6), linear shape of the H/D exchange was still unclear.

3.3. H/D exchange of [C_5mim][TFSI]- and [C_6mim][TFSI]-2-PrOD-d_8

The 2-PrOD-d_8 concentration dependence of the Raman bands obtained for [C_5mim][TFSI] is shown in Fig. 8. At < 80 mol%, C(2)-D Raman band was not observed; therefore, the H/D exchange was not activated in the propanol-poor region. At 80 mol%, the C(2)-D Raman band appeared and the C(2)-H Raman intensity decreased. After comparison with other f_D shapes [23], [C_5mim][TFSI]-2-PrOD-d_8 was classified as a combination of none (f_D = 0) and linear shape. Although the H/D exchange of [C_4mim][PF_6]-D_2O occurred at the water-poor region due to phase separation [23], the linear shape of f_D in [C_5mim][TFSI]-2-PrOD-d_8 was formed in the propanol-rich region (Fig. 4). Consequently, the combined f_D (constant + linear) is considered as a new f_D shape (Table 1). The systems in the [C_4mim][TFSI]- and [C_5mim][TFSI]-based mixtures were resolved in the entire propanol concentration region [30] and their nanoheterogeneities were similar [33]. In the same manner with linear shape of [C_4mim][TFSI]-2-PrOD-d_8, partial linear shape of

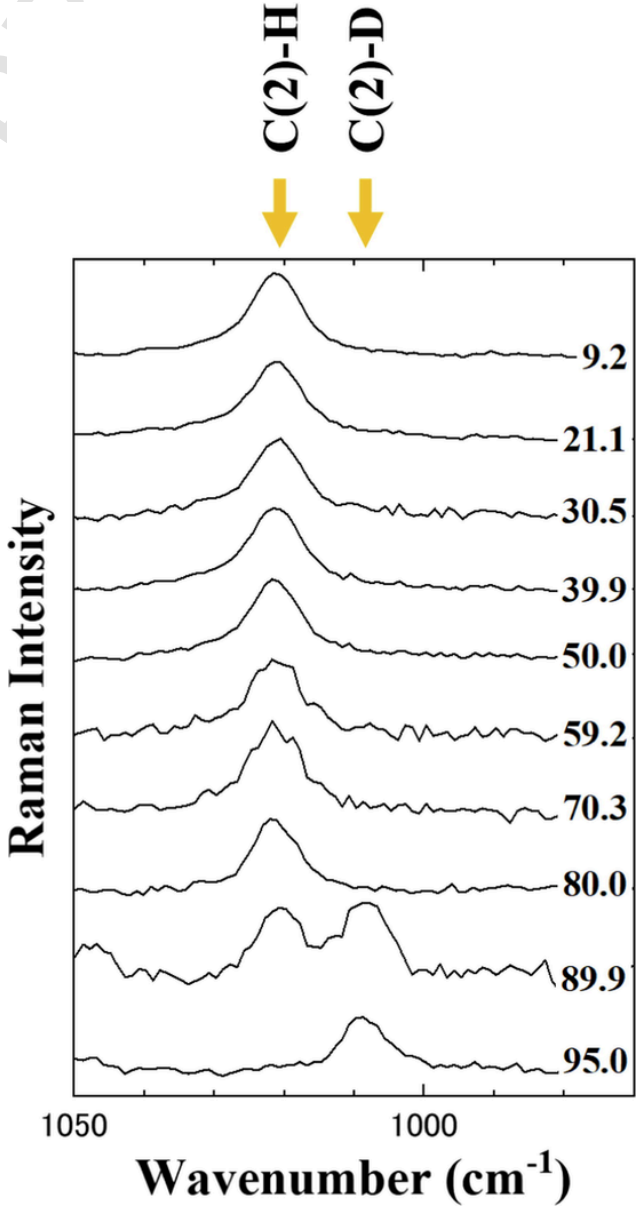

Fig. 8. H/D exchange on the Raman bands of [C_5mim][TFSI]-2-PrOD-d_8. These Raman bands are indicated by the arrows. Numbers in the figure reveal × mol% 2-PrOD-d_8.

f_D in [C5mim][TFSI]-2-PrOD-d8 could be modified by some additional factor, which is different from the nanoheterogeneous liquid structures.

The effect of solvent concentration in [C_6mim][TFSI]-2-PrOD-d_8 to the Raman bands were similar as shown in Fig. S3. At 2-PrOD-d_8 concentrations of > 80 mol%, the C(2)-D Raman band behaved similarly to the [C_5mim][TFSI]-based mixtures. The f_D curves shown in Fig. 4 suggest a similar behavior in the H/D exchange of both [C_5mim][TFSI]- and [C_6mim][TFSI]-based mixtures. Thus, [C_5mim][TFSI]-2-PrOD-d_8 and [C_6mim][TFSI]-2-PrOD-d_8 belong to the same H/D exchange group. The new type of f_D curve with propanol suggests that the H/D exchange mechanism in the [$C_n$mim][TFSI]-2-PrOD-d_8 system was quite complicated.

3.4. Kinetic H/D exchange of [C_6mim][TFSI]-MeOD-d_4, -acetone-d_6 and −2-PrOD-d_8

The kinetic isotope effect is a clue to interpret H/D exchange mechanism by the observed exchange rates [39–42]. Thus, we measured time-resolved Raman spectra at room temperature. Furthermore, additive effect for the H/D exchange is indispensable for the HDX-MS applications. For instance, in hydrophobic proteins, deuterated alcohol additives are necessary for the H/D exchange.

Fig. 9 reveals kinetic f_D of [C_6mim][TFSI]-90 mol% MeOD-d_4, −90 mol% acetone-d_6, and −90 mol% 2-PrOD-d_8. Obviously, acetone-d_6 cannot activate the H/D exchange even after 334hrs. In the ILs, acetone was found to be strong hydrogen bonding acceptor [43]. COSMO-RS calculations predicted that − O − of atom of the acetone is attractive to hydrogen of C(2)-H. Also, NMR experiments using [C_4mim][TFSI]-acetone supported the strong hydrogen bond acceptor character [43]. − O − of atom of the acetone could be preferred to bond to hydrogen of C(2)-H, and deuterium of acetone has a little probability to exchange with hydrogen of C(2)-H. Theoretical and experimental facts in [$C_n$mim][TFSI]-acetone did not contradict with no H/D exchange in [C_6mim][TFSI]-90 mol% acetone-d_6 for 334hrs.

Slow H/D exchange of [C_6mim][TFSI]-90 mol% MeOD-d_4 and −90 mol% 2-PrOD-d_8 was observed at room temperature (Fig. 9). Before starting the H/D exchange, incubation time, t_{inc}, was observed. Here, the incubation time is waiting time to start the H/D exchange and t_{inc} is originated from the activation energy [44]. Since t_{inc} was comparable in both systems, activation energy could be almost the same. However, H/D exchange rate of the MeOD-d_4-based mixture was greater than that of 2-PrOD-d_8-based one. Generally, upper critical solution temperature (UCST) in the LLE indicates the solubility in the mixture. The UCSTs were determined in the various IL-alcohol mixtures [30,31,34,45,46,47]. By changing anions, [C_2mim][TFSI]-alcohol mixtures indicated high solubility (lower UCST point) [46]. This means that the weaker interactions between [TFSI]$^-$ anion the solvent are induced. Alcohol molecules could prefer to stay in the cation site. Hence, the [TFSI]$^-$ anion can indirectly promote the H/D exchange of [C_6mim]$^+$ cation and alcohols. Considering the LLEs of [C_6mim][TFSI]-alcohol [45], the effect of the length of the alkyl chain on the alcohol was clearly observed. When the length of the alkyl chain on the alcohol decreases, solubility increases. Hence, it is interpreted that well-dissolved MeOD-d_4 can promote the H/D exchange.

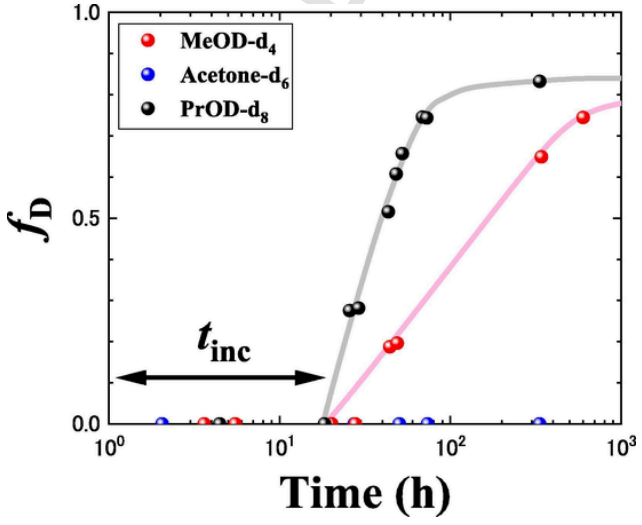

Fig. 9. H/D exchange fraction, f_D, as a function of time in [C_6mim][TFSI]-90 mol% MeOD-d_4, −90 mol% acetone-d_6, and −90 mol% 2-PrOD-d_8. The curves in the figure are guide for the eye.

4. Conclusions

The cation effect in H/D exchange of hydrophobic IL-propanol solutions was studied by Raman spectroscopy. In addition to an anion effect for H/D exchange using [C_4mim][X]-D_2O, [$C_n$mim][TFSI]-2-PrOD-d_8 solutions indicated a variety of H/D exchanges, which are based on a cation effect. The H/D exchange behaviors were not explained by the alkyl chain length of [$C_n$mim]$^+$. The H/D exchange fraction or f_D plots with different concentrations of propanol provided insights on the H/D exchange reaction process. [C_2mim][TFSI]-2-PrOD-d_8 showed no H/D exchange as described by the constant $f_D = 0$ at all the concentrations studied. [C_4mim][TFSI]-2-PrOD-d_8 provided the complicated H/D exchange behaviors; (i) linear f_D (linear shape), (ii) extended-N shape of [C_4mim]$^+$ conformers, and (iii) little anion contribution for H/D exchange. Kinetic H/D exchange can extract the activation energy, the H/D exchange rate, and additive effect.

CRediT authorship contribution statement

Hiroshi Abe: Conceptualization. **Yuto Yoshiichi:** Data curation. **Hiroaki Kishimura:** Data curation.

Declaration of Competing Interest

The authors declare that they have no known competing financial interests or personal relationships that could have appeared to influence the work reported in this paper.

Acknowledgments

We thank Mr. T. Hirano, Mr. T. Ohkubo, Dr. T. Takekiyo and Professor Y. Yoshimura of the National Defense Academy and Professor A. Shimizu of Soka University for experimental supports and helpful discussions.

References

[1] T. Li, J.E. Johnson, G.J. Thomas Jr, Raman Dynamic Probe of Hydrogen Exchange in Bean Pod Mottle Virus: Base-specific Retardation of Exchange in Packaged ssRNA, Biophys. J. 65 (1993) 1963–1972.
[2] R. Gremaud, Z. Łodziana, P. Hug, B. Willenberg, A.-M. Racu, J. Schoenes, A.J. Ramirez-Cuesta, S.J. Clark, K. Refson, A. Züttel, A. Borgschulte, Evidence for hydrogen transport in deuterated $LiBH_4$ from low-temperature Raman-scattering measurements and first-principles calculations, Phys. Rev. B 80 (2009) 100301–100304.
[3] M.G. Prechtl, M. Hölscher, Y. Ben-David, N. Theyssen, R. Loschen, D. Milstein, W. Leitner, H/D Exchange at Aromatic and Heteroaromatic Hydrocarbons Using D_2O as the Deuterium Source and Ruthenium Dihydrogen Complexes as the Catalyst, Angew. Chem. Int. Ed. 46 (13) (2007) 2269–2272.
[4] A. Dirvanauskas, R. Galavotti, A. Lunghi, A. Nicolini, F. Roncaglia, F. Totti, A. Cornia, Solution structure of a pentachromium(II) single molecule magnet from DFT calculations, isotopic labelling and multinuclear NMR spectroscopy, Dalton Trans. 47 (2018) 585–595.
[5] C. Gessner, W. Steinchen, S. Bédard, J.J. Skinner, V.L. Woods, T.J. Walsh, G. Bange, D.P. Pantazatos, Computational method allowing Hydrogen-Deuterium Exchange Mass Spectrometry at single amide Resolution, Sci. Rep. 7 (2017) 3789–3810.
[6] X. Lou, R.P.M. Lafleur, C.M.A. Leenders, S.M.C. Schoenmakers, N.M. Matsumoto, M.B. Baker, J.L.J. van Dongen, A.R.A. Palmans, E.W. Meijer, Dynamic diversity of

PROOF

synthetic supramolecular polymers in water as revealed by hydrogen/deuterium exchange, Nature Commun. 8 (2017) 15420–15428.
[7] R. Jia, C. Martens, M. Shekhar, S. Pant, G.A. Pellowe, A.M. Lau, H.E. Findlay, N.J. Harris, E. Tajkhorshid, P.J. Booth, A. Politis, Hydrogen-deuterium exchange mass spectrometry captures distinct dynamics upon substrate and inhibitor binding to a transporter, Nature Commun. 11 (2020) 6162–6210.
[8] J. Zhang, J.L. Balsbaugh, S. Gao, N.G. Ahn, J.P. Klinman, Hydrogen deuterium exchange defines catalytically linked regions of protein flexibility in the catechol O-methyltransferase reaction, Proc. Nat. Acad. Soc. 117 (20) (2020) 10797–10805.
[9] E.I. James, T.A. Murphree, C. Vorauer, J.R. Engen, M. Guttman, Chem. Rev. 122 (2022) 7562–7623.
[10] L.A. Blanchard, D. Hancu, E.J. Beckman, J.F. Brennecke, Green processing using ionic liquids and CO_2, Nature 399 (6731) (1999) 28–29.
[11] J.F. Brennecke, B.E. Gurkan, Ionic Liquids for CO_2 Capture and Emission Reduction, J. Phys. Chem. Lett. 1 (24) (2010) 3459–3464.
[12] T. Welton, Room-Temperature Ionic Liquids. Solvents for Synthesis and Catalysis, Chem. Rev. 99 (1999) 2071–2083.
[13] W. Leitner, A greener solution, Nature 423 (6943) (2003) 930–931.
[14] J.-P. Belieres, D. Gervasio, C.A. Angell, Binary inorganic salt mixtures as high conductivity liquid electrolytes for > 100 C° fuel cells, Chem. Commun. 4799–4801 (2006).
[15] M. Armand, F. Endres, D.R. MacFarlane, H. Ohno, B. Scrosati, Ionic-liquid materials for the electrochemical challenges of the future, Nature Mater. 8 (8) (2009) 621–629.
[16] T. Yasuda, M. Watanabe, Protic ionic liquids: Fuel cell applications, MRS Bull. 38 (2013) 560–566.
[17] S.T. Handy, M. Okello, The 2-Position of Imidazolium Ionic Liquids: Substitution and Exchange, J. Org. Chem. 70 (2005) 1915–1918.
[18] Y. Yasaka, C. Wakai, N. Matubayasi, M. Nakahara, Slowdown of H/D Exchange Reaction Rate and Water Dynamics in Ionic Liquids: Deactivation of Solitary Water Solvated by Small Anions in 1-Butyl-3-Methyl-Imidazolium Chloride, J. Phys. Chem. A 111 (2007) 541–543.
[19] R.C. Remsing, J.L. Wildin, A.L. Rapp, G. Moyna, Hydrogen Bonds in Ionic Liquids Revisited: $^{35/37}$Cl NMR Studies of Deuterium Isotope Effects in 1-n-Butyl-3-Methylimidazolium Chloride, J. Phys. Chem. B 111 (2007) 11619–11621.
[20] S. Ohta, A. Shimizu, Y. Imai, H. Abe, N. Hatano, Y. Yoshimura, Peculiar Concentration Dependence of H/D Exchange Reaction in 1-Butyl-3-methylimidazolium Tetrafluoroborate-D_2O Mixtures, Open, J. Phys. Chem. 1 (2011) 70–76.
[21] N. Hatano, M. Watanabe, T. Takekiyo, H. Abe, Y. Yoshimura, Anomalous Conformational Change in 1-Butyl-3-methylimidazolium Tetrafluoroborate–D_2O Mixtures, J. Phys. Chem. A 116 (2012) 1208–1212.
[22] V. Klimavicius, Z. Gdaniec, J. Kausteklis, V. Aleksa, K. Aidas, V. Balevicius, NMR and Raman Spectroscopy Monitoring of Proton/Deuteron Exchange in Aqueous Solutions of Ionic Liquids Forming Hydrogen Bond: A Role of Anions, Self-Aggregation, and Mesophase Formation, J. Phys. Chem. B 117 (2013) 10211–10220.
[23] Y. Yoshimura, N. Hatano, T. Takekiyo, H. Abe, Direct Correlation Between the H/D Exchange Reaction and Conformational Changes of the Cation in Imidazolium-Based Ionic Liquid–D_2O Mixtures, J Sol. Chem. 43 (9–10) (2014) 1509–1518.
[24] M. Zanatta, F.P. dos Santos, C. Biehl, G. Marin, G. Ebeling, P.A. Netz, J. Dupont, Organocatalytic Imidazolium Ionic Liquids H/D Exchange Catalysts, J. Org. Chem. 82 (2017) 2622–2629.
[25] A.E. Khudozhitkov, J. Neumann, T. Niemann, D. Zaitsau, P. Stange, D. Paschek, A.G. Stepanov, D.I. Kolokolov, R. Ludwig, Hydrogen Bonding Between Ions of Like Charge in Ionic Liquids Characterized by NMR Deuteron Quadrupole Coupling Constants—Comparison with Salt Bridges and Molecular Systems, Angew. Chem. Int. Ed. 58 (49) (2019) 17863–17871.
[26] Y. Yoshimura, T. Mori, K. Kaneko, K. Nogami, T. Takekiyo, Y. Masuda, A. Shimizu, Confirmation of local water structure confined in ionic liquids using H/D exchange, J. Mol. Liq. 286 (2019) 110874–110877.
[27] A.A. Shahkhatuni, A.G. Shahkhatuni, S.S. Mamyan, V.P. Ananikov, A.S. Harutyunyan, Proton–deuterium exchange of acetone catalyzed in imidazolium-based ionic liquid–D_2O mixtures, RSC Adv. 10 (54) (2020) 32485–32489.
[28] H. Abe, Y. Yoshiichi, H. Kishimura, Hydrogen bonding of nanoconfined water in ionic liquids, submitted to J. Phys. Chem. B.
[29] J. Kausteklis, M. Talaikis, V. Aleksa, V. Balevičius, Raman spectroscopy study of water confinement in ionic liquid 1-butyl-3-methylimidzolium nitrate, J. Mol. Liq. 271 (2018) 747–755.
[30] S. Ozawa, H. Kishimura, S. Kitahira, K. Tamatani, K. Hirayama, H. Abe, Y. Yoshimura, Isomer effect of propanol on liquid–liquid equilibrium in hydrophobic room-temperature ionic liquids, Chem. Phys. Lett. 613 (2014) 122–126.
[31] H. Abe, R. Fukushima, M. Onji, K. Hirayama, H. Kishimura, Y. Yoshimura, S. Ozawa, Two-length scale description of hydrophobic room-temperature ionic liquid–alcohol systems, J. Mol. Liq. 215 (2016) 417–422.
[32] O. Russina, A. Triolo, L. Gontrani, R. Caminiti, D. Xiao, L.G. Hines Jr, R.A. Bartsch, E.L. Quitevis, N. Plechkova, K.R. Seddon, Morphology and intermolecular dynamics of 1-alkyl-3-methylimidazolium bis{(trifluoromethane)sulfonyl}amide ionic liquids: structural and dynamic evidence of nanoscale segregation, J. Phys.: Condens. Matter 21 (2009) 424121–424129.
[33] H. Abe, F. Nemoto, S. Ozawa, Critical Scattering in Room-Temperature Ionic Liquid-Propanol Solutions, J. Sol. Chem. 50 (2) (2021) 220–231.
[34] H. Abe, E. Kohki, A. Nakada, H. Kishimura, Phase behavior in quaternary ammonium ionic liquid-propanol solutions: Hydrophobicity, molecular conformations, and isomer effects, Chem. Phys. 491 (2017) 136–142.
[35] L. Almásy, M. Turmine, A. Perera, Structure of Aqueous Solutions of Ionic Liquid 1-Butyl-3-methylimidazolium Tetrafluoroborate by Small-Angle Neutron Scattering, J. Phys. Chem. B 112 (8) (2008) 2382–2387.
[36] J.C. Lasse‘ gues, J. Grondin, R. Holomb, P. Johansson, J. Raman Spectrosc. 38 (2007) 551–558.
[37] H. Kishimura, E. Kohki, A. Nakada, K. Tamatani, H. Abe, Ether bond effects in quaternary ammonium and phosphonium ionic liquid-propanol solutions, Chem. Phys. 502 (2018) 87–95.
[38] F. Capitani, F. Trequattrini, O. Palumbo, A. Paolone, P. Postorino, Phase Transitions of PYR_{14}-TFSI as a Function of Pressure and Temperature: the Competition between Smaller Volume and Lower Energy Conformer, J. Phys. Chem. B 120 (2016) 2921–2928.
[39] F.H. Westheimer, The Magnitude of the Primary Kinetic Isotope Effect for Compounds of Hydrogen and Deuterium, Chem. Rev. 61 (3) (1961) 265–273.
[40] J. Szydłowski, Isotope effects on phase equilibria in hydrogen bonded systems, especially vapor pressure and miscibility isotope effects, J. Mol. Str. 321 (1–2) (1994) 101–113.
[41] R.L. Bell, T.N. Truong, Primary and Solvent Kinetic Isotope Effects in the Water-Assisted Tautomerization of Formamidine: An ab Initio Direct Dynamics Study, J. Phys. Chem. A 101 (1997) 7802–7808.
[42] E. Canet, D. Mammoli, P. Kaderˇávek, P. Pelupessy, G. Bodenhausen, Kinetic isotope effects for fast deuterium and proton exchange rates, Phys. Chem. Chem. Phys. 18 (2016) 10144–10151.
[43] E. Ruiz, V.R. Ferro, J. Palomar, J. Ortega, J.J. Rodriguez, Interactions of Ionic Liquids and Acetone: Thermodynamic Properties, Quantum-Chemical Calculations, and NMR Analysis, J. Phys. Chem. B 117 (2013) 7388–7398.
[44] H. Abe, M. Ishibashi, K. Ohshima, T. Suzuki, M. Wuttig, K. Kakurai, Kinetics of the martensitic transition in In-Tl alloys, Phys. Rev. B 50 (1994) 9020–9024.
[45] J.M. Crosthwaite, S.N.V.K. Aki, E.J. Maginn, J.F. Brennecke, Liquid phase behavior of imidazolium-based ionic liquids with alcohols: effect of hydrogen bonding and non-polar interactions, Fluid Phase Equilib. 228–229 (2005) 303–309.
[46] U. Domańska, Solubilities and thermophysical properties of ionic liquids, Pure Appl. Chem. 77 (2005) 543–557.
[47] A. Makowska, E. Dyoniziak, A. Siporska, J. Szydłowski, Miscibility of Ionic Liquids with Polyhydric Alcohols, J. Phys. Chem. B 114 (2010) 2504–2508.

CORRECTED PROOF